Contents lists available at ScienceDirect

Intelligent Medicine

journal homepage: www.elsevier.com/locate/imed

Review

Artificial intelligence-based medical image segmentation for 3D printing and naked eye 3D visualization

Guang Jia [1,*], Xunan Huang [1], Sen Tao [1], Xianghuai Zhang [1], Yue Zhao [1], Hongcai Wang [2], Jie He [2], Jiaxue Hao [1], Bo Liu [1], Jiejing Zhou [3], Tanping Li [4], Xiaoling Zhang [5], Jinglong Gao [5,*]

[1] School of Computer Science and Technology, Xidian University, Xi'an, Shaanxi 710068, China
[2] Shaanxi Xinweitai Biological Technology Co., Ltd., Xi'an, Shaanxi 710065, China
[3] Department of Radiation Oncology, Tangdu Hospital Affiliated to Air Force Medical University, Xi'an, Shaanxi 710071, China
[4] School of Physics and Optoelectronic Engineering, Xidian University, Xi'an, Shaanxi 710071, China
[5] Shaanxi Provincial People's Hospital, Xi'an , Shaanxi 710068, China

ARTICLE INFO

ABSTRACT

Image segmentation for 3D printing and 3D visualization has become an essential component in many fields of medical research, teaching, and clinical practice. Medical image segmentation requires sophisticated computerized quantifications and visualization tools. Recently, with the development of artificial intelligence (AI) technology, tumors or organs can be quickly and accurately detected and automatically contoured from medical images. This paper introduces a platform-independent, multi-modality image registration, segmentation, and 3D visualization program, named artificial intelligence-based medical image segmentation for 3D printing and naked eye 3D visualization (AIMIS3D). YOLOV3 algorithm was used to recognize prostate organ from T2-weighted MRI images with proper training. Prostate cancer and bladder cancer were segmented based on U-net from MRI images. CT images of osteosarcoma were loaded into the platform for the segmentation of lumbar spine, osteosarcoma, vessels, and local nerves for 3D printing. Breast displacement during each radiation therapy was quantitatively evaluated by automatically identifying the position of the 3D printed plastic breast bra. Brain vessel from multi-modality MRI images was segmented by using model-based transfer learning for 3D printing and naked eye 3D visualization in AIMIS3D platform.

1. Introduction

How to apply AI technology to detect diseases has attracted more and more attention [1–2]. Stanford University used AI to diagnose skin cancer with an accuracy rate of 91% [3]. Google has developed an augmented reality microscope (ARM) that aids in the detection of cancer. Because of the complexity and diversity of cancer diseases, using AI has a long way to go [4]. In this work, we developed artificial intelligence-based medical image segmentation for 3D printing and naked eye 3D visualization (AIMIS3D) by integrating AI technology into medical image analysis for automated organ segmentation. For example, prostate [5], bladder [6], spine [7], eyeball can be automatically contoured by using a convolutional neural networks (CNN) algorithm [8]. The automatically delineated organ border from each 2D cross-sectional image can be combined as a 3D object for 3D visualization and 3D printing.

AIMIS3D platform integrated with naked eye 3D visualization may improve the efficiency of communication among clinical doctors, who may use our interactive naked eye 3D visualization system to discuss a patient's disease and to optimize treatment planning. The doctors may sit around the visualization system and see a patient's internal 3D organs from different viewing angles without wearing any virtual reality (VR) glasses [9]. Each doctor may rotate, translate, or zoom in/out the 3D objects, and make annotations or marks by using either hand gesture recognition or voice control [10]. Naked eye 3D visualization system may facilitate doctor's ability to explain the details of the disease to patients [11].

2. Program design

AIMIS3D platform, written in the interactive data language (IDL) programming language, is modular in design, and takes advantage of IDL's object-oriented features and ready-to-use image processing functions. A functional overview and its core feature is diagrammed in Figure 1. The bottom block lists a subset of currently supported 2D cross-sectional image formats. Using information stored in the digital imaging

Figure 1. Functional overview of AIMIS3D's design. AIMI3D: artificial intelligence-based medical image segmentation for 3D printing and naked eye 3D visualization; DICOM: digital imaging and communications in medicine.

and communications in medicine (DICOM) file header, medical images are read into the 3D isotropic data buffer (such as $256 \times 256 \times 256$ or $512 \times 512 \times 512$), which can be processed to generate 3D polygon objects. The 3D object can have different types, such as IDLgrPolygon object, 3D mask with matrix size of $256 \times 256 \times 256$ or $512 \times 512 \times 512$, STL file, SAV file, or WRL file. Two functional blocks interface with the 3D objects and 3D isotropic data buffer: the Visualization and Algorithms. The "Visualization" interface provides the user with a graphical user interface to view and modify the 3D objects, to export STL files for 3D printing, and to generate four viewing angles for naked eye 3D visualization. The "Algorithms" module contains AI-based 3D image segmentation, 3D object splitting and modification, and vessel thickness measurement tools. The functionality of these tools is distributed over an intuitive user interface.

AIMIS3D platform is mainly composed of two windows: Load window and Modify window (Figure 2). The Load window allows user to preprocess DICOM images by using DICOM crawler, to load DICOM images for an automatic segmentation of 3D objects, and to open STL files for 3D visualization. One or multiple 3D objects could be selected and modified by going into the modify window. A user could do all sorts of manipulations to the selected 3D objects and use naked eye 3D visualization to see the whole process from four viewpoints (front, back, left, and right) by using the naked eye 3D projection hardware.

AIMIS3D enables the loading of multi-modality images for registration and comparison. The image registration algorithm is based on mutual information and Gaussian pyramid. The registration process not only considers the correlation of gray level information, but also uses Gaussian pyramid to improve the registration efficiency, which improves the registration accuracy layer by layer from coarse resolution to fine resolution image (Figure 3). The orthogonal views from multi-modality images can be combined with segmentation result visualization for interactive distance or angle measurements.

AI-based segmentation in AIMIS3D platform uses deep convolutional neural network (DCNN) to automatically extract organ border and tumor border [12]. DCNN is an emerging form of computer-aided design (CAD) analysis that allows for the automatic extraction of features and the supervision of large amounts of data to form quantitative decisions [13]. There is growing evidence that deep learning analysis may be a potential alternative to traditional handcrafted methods for pattern recognition and imaging classification problems. However, the focus of research is on combining DCNN and multiparameter MRI to address lesion detection and classification. Le et al. [14] used T2-weighted, apparent diffusion coefficient (ADC) and their combinations as inputs to explore three traditional DCNN models (VGG Net, Google Net and ResNet) [15]. The enhancement method was used to increase the number of samples in the training data set. Liu et al [16] proposed XmasNet inspired by VGG Net. Batch normalization was added after convolution to accelerate convergence during backpropagation. In these studies, patches (square regions) were extracted from the image as input to the DCNN model
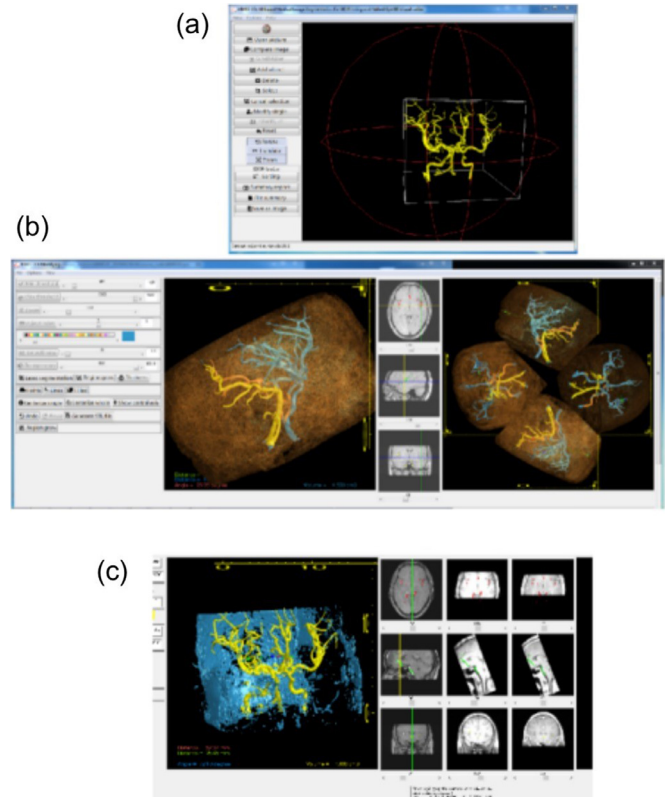
Figure 2. Two windows, load window (a) and modify window (b), were designed. The modify window has three orthogonal views and four-angle views for naked eye 3D visualization. Multi-modality images can be loaded in load window and registered for comparison in modify window (c).
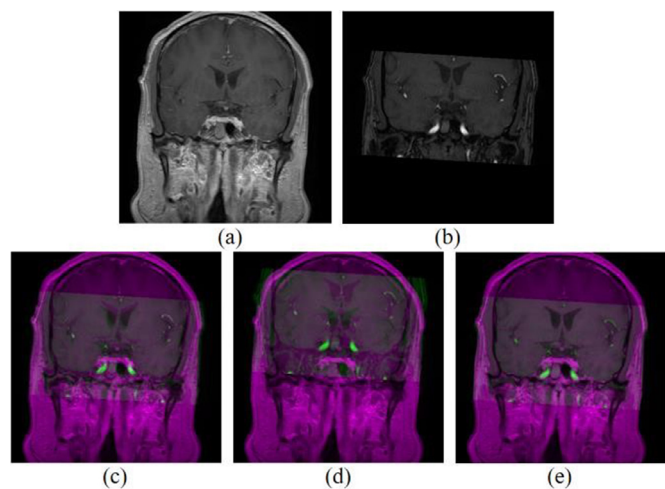
Figure 3. Multi-modality image registration. The reference image (a) and original unregistered image (b) can be registered and overlapped based on DICOM image orientation label information (c), based on mutual information (d), and based on mutual information and Gaussian pyramid (e).

to help the DCNN focus on the number of regions of interest (ROI), multiparametric-MR images, and to increase the number of samples in the data set.

AIMIS3D platform can be embedded into a naked eye 3D visualization system. The four viewing angels (front, back, left, and right) are patched together and projected to a screen. A flipped pyramid-shaped plastic/glass frame covered with holographic film can reflect each viewpoint to the eyes of the surrounding audiences. For mixed re-
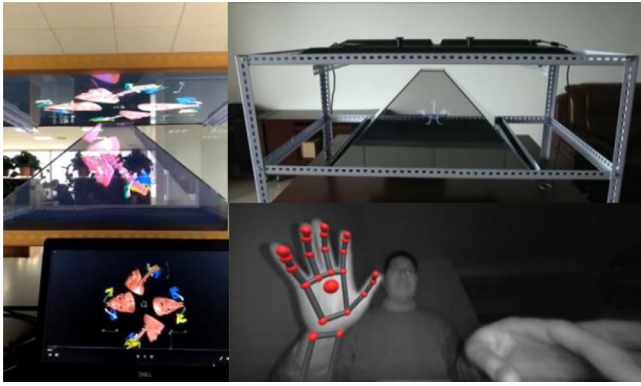
Figure 4. Naked eye 3D holographic projection system was built by using a mini-holographic projection user client system from with hand gesture recognition and control.
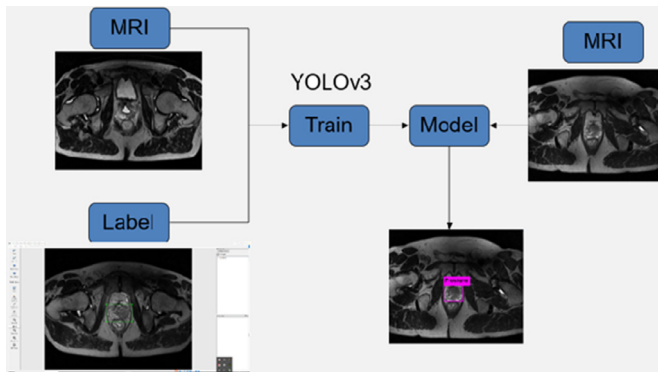

Figure 5. Prostate detection based on YOLOV3 algorithm.

ality, HoloLens depth camera can capture and recognize hand gesture, which can be used to control the displayed 3D objects in combination with voice control. 3D objects can be rotated, translated, zoomed, measured, and marked by voice control and hand gesture recognition. The naked eye 3D visualization supports multiple users to share and simultaneously manipulate 3D objects. A user client system installed in a cell phone or an iPad allows user to view 3D objects via a mini-holographic projection system (Figure 4).

3. Clinical applications

3.1. Prostate cancer MRI analysis

One of the hot topics in recent years is using convolutional neural networks to segment organs and detect cancer [17–20]. Li et al. used YOLOV3 algorithm to locate carotid artery and detect lesions on three-dimensional MRI. YOLO outperforms the detection methods in a smoothing way from others like Medical image DPM, SSD, CNN and R-CNN [21]. Our platform has a built-in YOLOV3 algorithm that can be used to recognize organs from T2-weighted MRI images with proper training (Figure 5). Prostate data were downloaded from the I2CVB (http://i2cvb.github.io/#prostate-data). The data set consisted of a total of 19 patients, 17 of whom had biopsy-confirmed prostate cancer and 2 patients were negative for biopsy. T2-weighted MRI images and parameter maps (ADC and DCE) were rescaled to 8-bit grayscale image and combined into RGB color images as the components of red, green and blue respectively.

Take prostate for example, AI in prostate cancer detection has been making progress. In 2002, researchers prospectively developed an artificial neural network (ANN) to detect prostate cancer by early detection of male prostate specific antigen (PSA) levels [22–23]. Lemaitre et al.
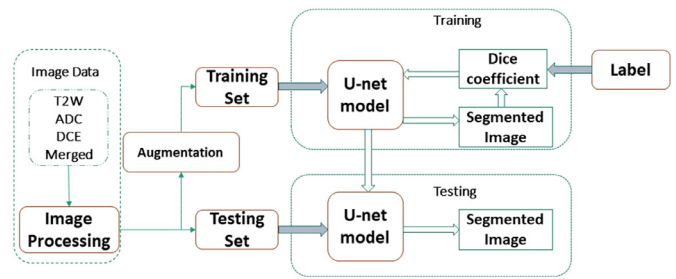

Figure 6. U-net algorithm was used to automatically detect prostate tumor borders.
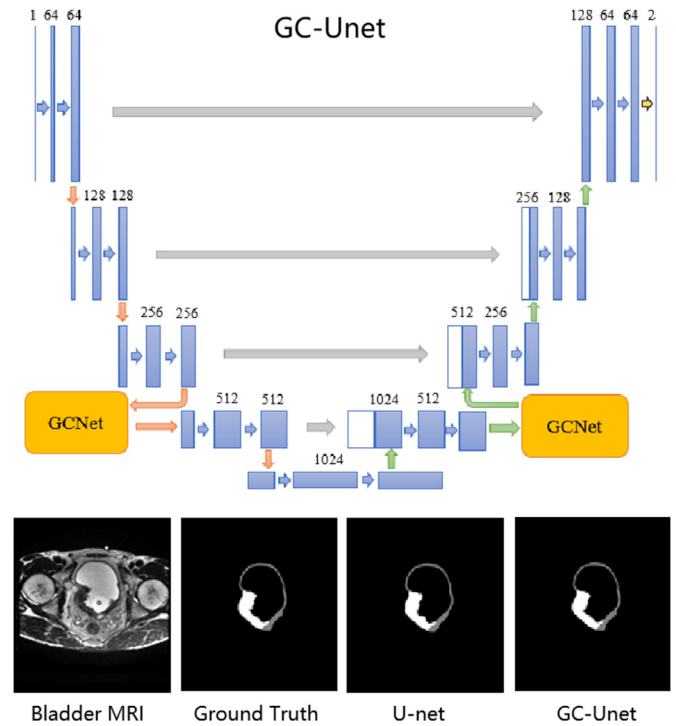

Figure 7. GC-Unet-based algorithm was used to detect bladder wall and tumor.

developed a computer-aided diagnosis system based on random forest to provide a probability map of prostate cancer location [24]. In the past two years, several computer-aided diagnostic systems for prostate cancer detection based on convolutional neural networks were developed for multi-parameter MRI [25–27].

The U-net algorithm was developed to detect prostate cancer masks based on T2-weighted MRI images and functional images (diffusion and perfusion MRI images) (Figure 6) [28]. Use the I2CVB data set mentioned above to do prostate cancer segmentation based on U-Net network. We randomly selected 13 out of 17 patients diagnosed with prostate cancer as the training set and the remaining cases as the test set. For T2-weighted sequence only, the segmentation accuracy is low, only 0.5877. ADC map only and DCE map only are better for prostate segmentation, and the accuracy is about 0.88. After the three parameter maps were combined into color images, the segmentation accuracy is 0.91.

3.2. Bladder cancer MRI analysis

Deep learning methods based on convolutional neural networks can be applied to T2-weighted MRI for automatic classification and segmentation of bladder cancer (Figure 7). Bladder cancer dataset was from ISICDM2019 bladder cancer segmentation challenge
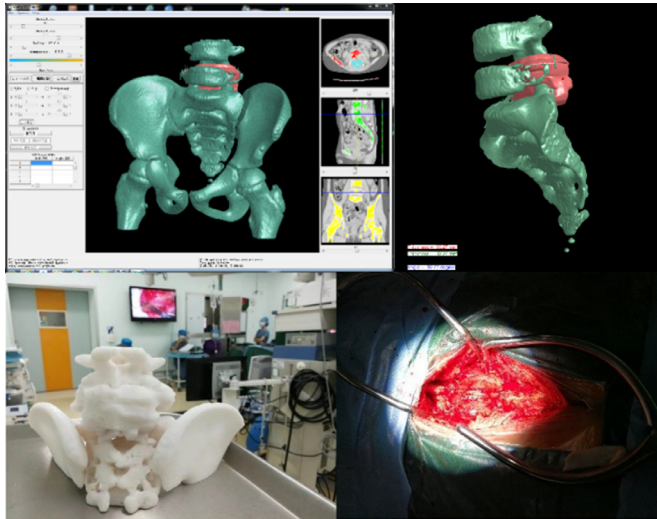
Figure 8. 3D printing of bony structure was used to assist the resection of lumbar osteosarcoma of an eight-year-old patient.

(http://www.imagecomputing.org/2019/challenge.html), in which a total of 2,000 T2-weighted MRI images of 38 bladder cancer cases were included. 794 images with tumor bearing were defined as positive samples and 1,206 images without tumor bearing as negative samples. The proportion of training, verification and test images is 7:2:1.

The Dice coefficient is 0.841 using U-net and 0.875 using GC-Unet. The sensitivity is 0.851 using U-net and 0.907 using GC-Unet. The specificity is 0.954 using U-net and 0.981 using GC-Unet.

3.3. Osteosarcoma visualization and 3D printing of CT images

Osteosarcoma is a kind of tumor with the highest malignancy among bone tumors and the highest incidence rate among orthopedic malignancies. The incidence rate of osteosarcoma is 1%–3%. 90% of osteosarcoma occurs in teenagers. The common incidence site of male is the metaphysis of the long shaft and mainly around the knee joint. Most of the tumors are found in the distal femur and proximal tibia.

CT images of osteosarcoma were loaded into the platform, in which the lumbar spine, osteosarcoma, vessels, and local nerves were separated and visualized as 3D objects. 3D printing of the lumbar spine could clearly show that tumor tissue infiltrates and lyses the bone cortex (Figure 8).

3.4. Breast cancer visualization and treatment response assessment of perfusion CT images

In radiation therapy of breast cancer, it is difficult to ensure that the patient's exposure position is identical and appropriate during every treatment. We conducted a study to determine whether 3D printing of a plastic breast bra could improve the accuracy of breast cancer's clinical radiation therapy.

Perfusion CT images of breast cancer during radiation therapy were analyzed by using 2-compartment pharmacokinetic modeling. Pharmacokinetic parameter mapping of breast cancer could be visualized in a 3D mode for therapy response assessment [29]. Changes of tumor volume and pharmacokinetic parameters could be evaluated [30].

During radiation therapy, it is crucial to accurately irradiate the tumor target position. However, the patient's position may change and the breast may shift to different positions during each treatment. 3D printing of a plastic breast bra was used to restrict breast motion and to minimize breast position change, which was quantitatively evaluated on CT images. CT images of patients with breast cancer were converted to 3D
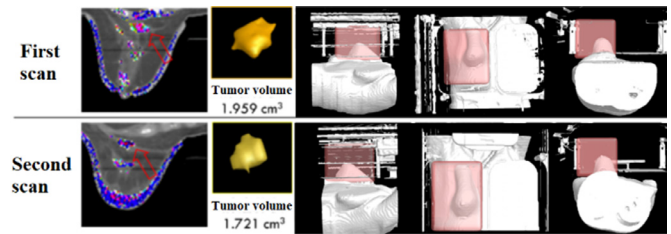
Figure 9. Tumor border was automatically delineated in order to monitor radiotherapy responses. The relative breast position changes between two radiation treatments were quantitatively evaluated.
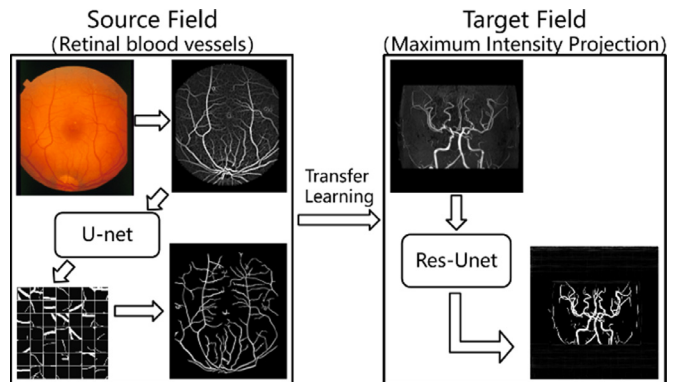
Figure 10. Brain vessels was segmented using transfer learning with U-net network.

objects. Breast displacement during each radiation therapy was quantitatively evaluated by automatically identifying the position of the 3D printed plastic breast bra (Figure 9).

3.5. Brain vessel 3D printing, and naked eye 3D visualization of time-of-flight MRI images

Cardiovascular and cerebrovascular disease has always been the severe problem faced by the patients in many countries and is a leading cause of mortality and morbidity. More and more evidence suggests that it is the ingredient of the vascular wall and stenosis degree of the lumina determining the vessel vulnerability.

A total of 6 cases with intracranial atherosclerosis were imaged at 3T MRI scanner at Shaanxi Provincial People's Hospital. The dataset is composed of 72 maximum intensity projection (MIP) images generated from time-of-flight MRI (Figure 10). Blood vessel exhibits a bright signal on time-of-flight MRI and was segmented by using Res-Unet-based transfer learning [31–32]. The proportion of training, verification and test images is 6:1:2. The Dice coefficient is 0.798 using U-net and 0.914 using Res-Unet. The accuracy was 0.849 using U-net and 0.906 using Res-Unet.

Key advantages of the AIMIS3D platform are that it utilizes morphological information, such as local wall thickness, and active contour of the aorta to limit the impact from noise and artifacts in MRI images. Thin vessels were labeled with red and yellow as a warning sign for atherosclerotic plaques (Figure 11).

Vessel wall MRI is a hot topic in detecting atherosclerotic disease [33] and evaluating the vulnerability of atherosclerotic plaques based on wall enhancement [34–35]. High-resolution MRI has demonstrated better potential in the identification of the components of atherosclerotic plaque, such as the fibrous cap (FC), intraplaque hemorrhage, calcification, and the lipid-rich, necrotic core, as well as quantifying plaque areas and volumes. Moreover, high-resolution MRI with a 3D time-of-flight protocol was capable of differentiating an intact, thick FC from an intact, thin, and ruptured cap. With the guidance of seg-
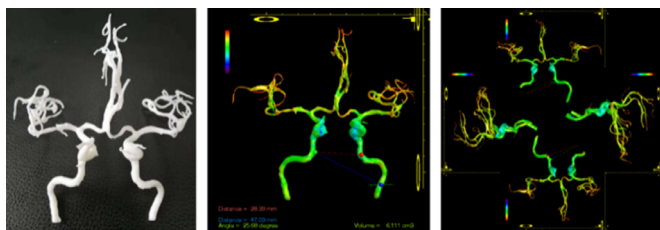
Figure 11. Segmented brain vessels were exported to STL file for 3D printing with nylon material (left). Vessel thickness was calculated and displayed with rainbow color bar (middle). Four views with front, back, left, right were composed together for naked eye 3D visualization (right).

mented blood vessels from time-of-flight MRI, flow void artifacts on post-contrast black-blood MRI could be removed and atherosclerotic plaques could be better visualized. AI algorithms on plaque detection and plaque vulnerability were trained by using intracranial plaque cases with Radiologist's labels [36].

4. Conclusions and future directions

Significant progress has been achieved in building a platform-independent, 3-dimensional, automated-segmentation, extensible image processing application. However, much work still remains to meet the broader needs of the clinical practice and 3D visualization environment.

A stand-alone runtime distribution of AIMIS3D can be created in IDL. The newest version and user manual have been uploaded to the public website for free usage and evaluation (A Collection of Chinese Medical Imaging AI Software, http://www.cvnis.net/caimi/index.html). AIMIS3D could be developed by other languages, such as Matlab. IDL has strong image processing capability and bridge technology that allow AIMIS3D software to share AI-based medical image segmentation information between IDL and other languages, such as Python and Java. The executable version of AI algorithm developed in Python can be executed through the SPAWN procedure in IDL for integration into AIMIS3D platform.

A variety of naked eye 3D visualization hardware was added with hand gesture and voice control. Future enhancements will also include AI-based disease delineation, a more complex AI algorithm for accurate organ and tumor segmentation, and the continuous modification of specialized components to address specific requirements identified by clinical physicians, such as ultrasound-based heart valve segmentation and perfusion CT-based breast tumor segmentation, and atherosclerotic plaque analysis. While AIMIS3D platform has primarily addressed radiological imaging modalities for 3D printing and naked eye 3D visualization, it is suitable for other types of datasets and applications, such as microarrays, microscopy images, micrographs, virtual reality, mixed reality, teaching, architecture, and industrial design. Future enhancements will add functionality for these technologies as required.

Conflicts of interest statement

The authors declare that there are no conflicts of interest.

Funding

Author contributions

References

[1] Amisha, Malik P, Pathania M, et al. Overview of artificial intelligence in medicine. J Family Med Prim Care 2019;8(7):2328–31. doi:10.4103/jfmpc.jfmpc_440_19.

[2] Mintz Y, Brodie R. Introduction to artificial intelligence in medicine. Minim Invasive Ther Allied Technol 2019;28(2):73–81. doi:10.1080/13645706.2019.1575882.

[3] Esteva A, Kuprel B, Novoa RA, et al. Dermatologist-level classification of skin cancer with deep neural networks. Nature 2017;542(7639):115–18. doi:10.1038/nature21056.

[4] Wu Y, Giger ML, Doi K, et al. Artificial neural networks in mammography: application to decision making in the diagnosis of breast cancer. Radiology 1993;187(1):81–7. doi:10.1148/radiology.187.1.8451441.

[5] Zhu Q, Du B, Turkbey B, et al. Deeply-supervised CNN for prostate segmentation. In: Proceedings of the international joint conference on neural networks. Anchorage, United States: IEEE; 2017.

[6] Samala RK, Chan HP, Caoili EM, et al. Urinary bladder segmentation in CT urography using deep-learning convolutional neural network and level sets. Med Phys 2016;43(4):1882. doi:10.1118/1.4944498.

[7] Liao H, Mesfin A, Luo J. Joint vertebrae identification and localization in spinal CT images by combining short- and long-range contextual information. IEEE Trans Med Imaging 2018;37(5):1266–75. doi:10.1109/TMI.2018.2798293.

[8] Krizhevsky A, Sutskever I, Hinton GE. Imagenet classification with deep convolutional neural networks. Adv Neural Inf Process Syst 2012;25(2). doi:10.1145/3065386.

[9] Kim Y, Kim H, Kim YO. Virtual reality and augmented reality in plastic surgery: a review. Arch Plast Surg 2017;44(3):179–87. doi:10.5999/aps.2017.44.3.179.

[10] Cheok MJ, Omar Z, Jaward MH. A review of hand gesture and sign language recognition techniques. Int J Mach Learn Cybern 2019;10(1):131–53.

[11] Wolf SM. Conflict between doctor and patient. Law Med Health Care 1988;16(3-4):197–203. doi:10.1111/j.1748-720x.1988.tb01946.x.

[12] Hu P, Wu F, Peng J, et al. Automatic abdominal multi-organ segmentation using deep convolutional neural network and time-implicit level sets. Int J Comput Assist Radiol Surg 2017;12(3):399–411. doi:10.1007/s11548-016-1501-5.

[13] Sun L, Wang J, Hu Z, et al. Multi-view convolutional neural networks for mammographic image classification. IEEE Access 2019:7. doi:10.1109/ACCESS.2019.2939167.

[14] Le MH, Chen J, Wang L, et al. Automated diagnosis of prostate cancer in multiparametric MRI based on multimodal convolutional neural networks. Phys Med Biol 2017;62(16):6497–514. doi:10.1088/1361-6560/aa7731.

[15] Moosavi Dezfooli SM, Fawzi A, Fawzi O, et al. Universal adversarial perturbations. In: Proceedings - 30th IEEE conference on computer vision and pattern recognition. Honolulu, United States: CVPR; 2017.

[16] Liu S, Zheng H, Feng Y, et al. Prostate cancer diagnosis using deep learning with 3D multiparametric MRI Progress in biomedical optics and imaging - proceedings of SPIE Orlando, United States; 2017. doi:101117/122277121.

[17] Zhu J, Zhang J, Qiu B, et al. Comparison of the automatic segmentation of multiple organs at risk in CT images of lung cancer between deep convolutional neural network-based and atlas-based techniques. Acta Oncol 2019;58(2):257–64. doi:10.1080/0284186X.2018.1529421.

[18] Men K, Dai J, Li Y. Automatic segmentation of the clinical target volume and organs at risk in the planning CT for rectal cancer using deep dilated convolutional neural networks. Med Phys 2017;44(12):6377–89. doi:10.1002/mp.12602.

[19] Mehdy MM, Ng PY, Shair EF, et al. Artificial neural networks in image processing for early detection of breast cancer. Comput Math Methods Med 2017;2017:2610628. doi:10.1155/2017/2610628.

[20] Shell J, Gregory WD. Efficient cancer detection using multiple neural networks. IEEE J Transl Eng Health Med 2017;5:2800607. doi:10.1109/JTEHM.2017.2757471.

[21] YOLO(You only look once) making object detection work in medical imaging on convolution detection system. Int J Pharmaceut Res 2020;12(2).

[22] Djavan B, Remzi M, Zlotta A, et al. Novel artificial neural network for early detection of prostate cancer. J Clin Oncol 2002;20(4):921–9. doi:10.1200/JCO.2002.20.4.921.

[23] Abraham P, Wilfred G. A massive increase in serum beta-glucuronidase after a single dose of carbon tetrachloride to the rat. Clin Chim Acta 2002;322(1-2):183–4. doi:10.1016/s0009-8981(02)00170-5.

[24] Vos PC, Barentsz JO, Karssemeijer N, et al. Automatic computer-aided detection of prostate cancer based on multiparametric magnetic resonance image analysis. Phys Med Biol 2012;57(6):1527–42. doi:10.1088/0031-9155/57/6/1527.

[25] Wang Z, Liu C, Cheng D, et al. Automated detection of clinically significant prostate cancer in mp-MRI images based on an end-to-end deep neural network. IEEE Trans Med Imaging 2018;37(5):1127–39. doi:10.1109/TMI.2017.2789181.

[26] Song Y, Zhang YD, Yan X, et al. Computer-aided diagnosis of prostate cancer using a deep convolutional neural network from multiparametric MRI. J Magn Reson Imaging 2018;48(6):1570–7. doi:10.1002/jmri.26047.

[27] Yang X, Liu C, Wang Z, et al. Co-trained convolutional neural networks for automated detection of prostate cancer in multi-parametric MRI. Med Image Anal 2017;42:212–27. doi:10.1016/j.media.2017.08.006.

[28] Dolz J, Xu X, Rony J, et al. Multiregion segmentation of bladder cancer structures in MRI with progressive dilated convolutional networks. Med Phys 2018;45(12):5482–93. doi:10.1002/mp.13240.

[29] Hoffmann U, Brix G, Knopp MV, et al. Pharmacokinetic mapping of the breast: a new method for dynamic MR mammography. Magn Reson Med 1995;33(4):506–14. doi:10.1002/mrm.1910330408.

[30] Yu HJ, Chen JH, Mehta RS, et al. MRI measurements of tumor size and pharmacokinetic parameters as early predictors of response in breast cancer patients undergoing neoadjuvant anthracycline chemotherapy. J Magn Reson Imaging 2007;26(3):615–23. doi:10.1002/jmri.21060.

[31] He K, Zhang X, Ren S, et al. Identity mappings in deep residual networks Identity mappings in deep residual networks; 2016. Amsterdam, Netherlands. doi:10.1007/978-3-319-46493-0_38.

[32] He K, Zhang X, Ren S, et al. Deep residual learning for image recognition. In: Proceedings of the IEEE computer society conference on computer vision and pattern recognition, Las Vegas, United States; 2016.

[33] Mossa-Basha M, de Havenon A, Becker KJ, et al. Added value of vessel wall magnetic resonance imaging in the differentiation of Moyamoya Vasculopathies in a non-Asian cohort. Stroke 2016;47(7):1782–8. doi:10.1161/STROKEAHA.116.013320.

[34] Botnar RM, Stuber M, Kissinger KV, et al. Noninvasive coronary vessel wall and plaque imaging with magnetic resonance imaging. Circulation 2000;102(21):2582–7. doi:10.1161/01.cir.102.21.2582.

[35] Aoki S, Shirouzu I, Sasaki Y, et al. Enhancement of the intracranial arterial wall at MR imaging: relationship to cerebral atherosclerosis. Radiology 1995;194(2):477–81. doi:10.1148/radiology.194.2.7824729.

[36] Kerwin W, Xu D, Liu F, et al. Magnetic resonance imaging of carotid atherosclerosis: plaque analysis. Top Magn Reson Imaging 2007;18(5):371–8. doi:10.1097/rmr.0b013e3181598d9d.